Tellus (2007), 59B, 625–632
Printed in Singapore. All rights reserved

TELLUS

Observational validation of an extended mosaic technique for capturing subgrid scale heterogeneity in a GCM

By HAYDEE SALMUN[1]*, ANDREA MOLOD[2] and ANDREEA IRA[1], [1]*Hunter College, The City University of New York, New York, NY, 10021, USA;* [2]*Massachusetts Institute of Technology, Cambridge, MA, 01239, USA*

(Manuscript received 30 April 2006; in final form 27 November 2006)

ABSTRACT

A technique called extended mosaic (EM) was designed to allow the subgrid scale interactions between the land surface and the atmosphere to extend vertically. EM addresses a limitation of previously existing techniques, and has been shown to have an important impact on the simulated climate in global models. The present work focuses on an observational validation of the climate characteristics of a general circulation model using EM, based on a set of 10-yr simulations with each of EM and the standard mosaic technique (M), driven by climatological sea surface temperatures. Model simulations using EM show improvements in many aspects of the mid-latitude climate and in wintertime air temperature over Alaska and Western Canada and in the pattern of the Australian monsoon precipitation over land. An example of a degradation in the EM simulation is the temperature over southern South America in wintertime.

1. Introduction

It is now well recognized that the simulation of land–atmosphere exchange processes in global climate models is an important element of the overall simulation and prediction of climate and climate change. The remaining difficulties in the accurate simulation of these processes were articulated in the 2001 International Panel on Climate Change report (IPCC, 2001), and point to, among other areas, the treatment of heterogeneous landscapes and the coupling between the land surface and boundary layer submodels within general circulation models (GCMs).

A technique called 'extended mosaic' (Molod et al., 2003) was developed to address the issue of modelling the coupling between the land surface and the boundary layer over heterogeneous terrain. Previously existing techniques included an implicit assumption that the 'blending height', the level at which the boundary layer is assumed horizontally homogeneous, is at or below the level of the surface layer, approximately 50 m above the surface. There exists ample *in situ* observational evidence, however, that horizontal heterogeneities in the boundary layer persist upward almost throughout the boundary layer depth. 'Extended mosaic' (EM) relaxes the assumption about the blending height, and allows the direct impact of subgrid scale variability to extend throughout the vertical extent of the planetary boundary layer where conditions dictate. EM follows the standard 'mosaic' (M) approach in that the surface energy equations are solved separately for each tile or vegetation type in a grid box, but allows for the vertical 'extension' by performing the entire turbulent boundary layer calculation separately for each tile as well. As in the mosaic approach, the tiles of the mosaic interact only through the influence on the grid scale atmospheric fields. EM, then, 'solves different boundary layers' for the different surface types within a grid box.

Molod et al. (2004) (hereafter, MSW04) showed that a GCM simulation using EM was significantly different from a simulation using the standard M technique. The differences were largest over the United States, Mongolia and South Africa in summertime, over the Australian monsoon, and the EM simulation showed a strengthened Pacific North America (PNA) pattern of variability. The study of EM–M differences provided some insight into the reasons for the significant differences, but provided no comparison with observations to indicate whether any of the differences represented an improved climate simulation. The present study evaluates a set of GCM experiments which compare EM, the standard Mosaic technique, M and observational estimates in order to make the determination of where and whether the EM technique constitutes an improvement in the modelling of the land–atmosphere coupling. In the next section, a brief summary of the model experiments and observational estimates used in this study are presented. Results of the intercomparison are presented and discussed in Section 3 and the study is summarized in Section 4.

*Corresponding author.
e-mail: hsalmun@earth.geo.hunter.cuny.edu
DOI: 10.1111/j.1600-0889.2007.00257.x

2. GCM Experiments and Observations

The experiments described here were designed to examine the impact on a GCM's climate of modelling the influence of subgrid scale heterogeneity in vegetation using the EM technique. Two 10-yr simulations were performed with the NASA Goddard GEOS-3 GCM, one coupling the turbulence and land surface schemes with EM and one using the standard mosaic (M) coupling. The M simulation was performed with a modified version of the EM code which explicitly aggregates the turbulent fluxes at the surface layer. Constructing the experiments in this manner assures that the *only* differences between the GCM simulations are due to the choice of the vertical level at which the turbulent fluxes are aggregated. Each simulation (EM and M) began with the same initial conditions, and the deep soil state was spun up from 8 yrs of assimilation with the GEOS data assimilation system (DAS) using EM. The surface vegetation distribution was specified from DeFries and Townshend (1994), the characteristics of the different vegetation types were specified from Dorman and Sellers (1989), and the boundary conditions at the sea surface (sea surface temperature, SST and sea ice extent) were specified from the 50-yr climatology of Reynolds (1988).

The comparisons of GCM and observations in the present study use the temperature and humidity in the boundary layer and the total precipitation. The 850 mb temperature and relative humidity fields are evaluated using NCEP/NCAR reanalysis data (Kalnay et al., 1996). The reanalysis uses a global data assimilation system, which combines data and models to provide a 'best linear unbiased estimate' of the state of the atmosphere. The horizontal resolution of the reanalysis is T62 (about 210 km). Reanalysis fields are classified into four classes, depending on the degree to which they are influenced by the observations and/or the model, and the fields used here for comparison are all directly analysed and therefore most directly constrained by observations.

The observational estimate for total precipitation is the Global Precipitation Climatology Project (GPCP) satellite-gauge precipitation product of Huffman et al. (1995). The precipitation estimate is a combination of microwave satellite data, infrared satellite data, rain gauge analyses, and numerical weather prediction models. The first step of the technique used to combine the various data sources is the development of a multi-satellite product using microwave and infrared at low latitudes, and microwave data alone at higher latitudes. The second step is the inclusion of the rain gauge analysis, weighting each field by its inverse relative error variance. Finally, ECMWF numerical model results are used to fill data voids in the combined satellite-gauge estimate.

3. Results and Discussion

The observational validation presented here will be focused on the differences between EM and M discussed in MSW04. That paper explains that the direct impact of EM on the boundary layer climate is to increase the subgrid scale variability throughout the boundary layer depth and so increase the turbulent kinetic energy (TKE) as well. In regions where the winds are relatively weak, and where the vegetation is characterized by a large degree of variability, the effects of this change in TKE and therefore in boundary layer turbulent diffusion are more apparent. The sign of the EM–M difference was shown in MSW04 to be related to the underlying climate, in particular to the local Bowen ratio, as that determines the relative importance of increased diffusion of moisture versus heat. A stronger influence of heat diffusion results in a warmer and drier EM climate, and a stronger influence of moisture diffusion results in a wetter and cooler EM climate.

The first focus of MSW04 is the summertime climate over certain mid-latitude land areas. The planetary boundary layer depth, sensible heat flux and canopy temperature were all found to be higher in EM over the eastern United States, southern Africa and southeast and northeast Asia, where the latent heat flux and the convective precipitation were lower. The reason for this behaviour was traced to the enhanced eddy diffusion EM relative to M as a direct result of the change in technique from EM to M. The higher eddy diffusion of heat and moisture resulted in a warmer boundary layer temperature, which resulted in a lower boundary layer relative humidity and the suppression of the precipitation. The lower precipitation resulted in drier soils and less evaporation, which acted to warm the canopy temperatures. The warmer skin temperatures, in turn, generated higher sensible heat flux and higher eddy diffusion. The GCM results were used to elucidate this behaviour, but the elements which can be verified observationally are the boundary layer temperature and relative humidity and the precipitation. The June–July–August (JJA) seasonal mean 850 mb temperature and relative humidity from the GCM and from the NCEP/NCAR reanalysis, and the total precipitation from the GCM and from the GPCP satellite-gauge estimate are presented below to determine the extent to which the summertime EM–M behaviour represents an improvement in EM relative to M.

Another of the main differences between simulations with EM and M reported in MSW04 was the strengthening of the PNA pattern of variability in the EM simulation. Although no direct mechanism for this behaviour was presented, other studies which suggest the possibility that land surface hydrology may exert a remote influence on the circulation were cited. The remote influence of the PNA on the wintertime temperature in western Canada and Alaska (Koide and Kodera, 1999) is the basis of the observational validation of the strengthened PNA that will be presented below, where we compare December– January–February (DJF) seasonal mean 850 mb temperatures among the two GCM simulations and the reanalysis.

Another focus of the analysis of EM–M differences reported in MSW04 is the region of the Australian monsoon. The EM simulation had larger precipitation amounts over the northern land areas, and less over the ocean. This constitutes an increased

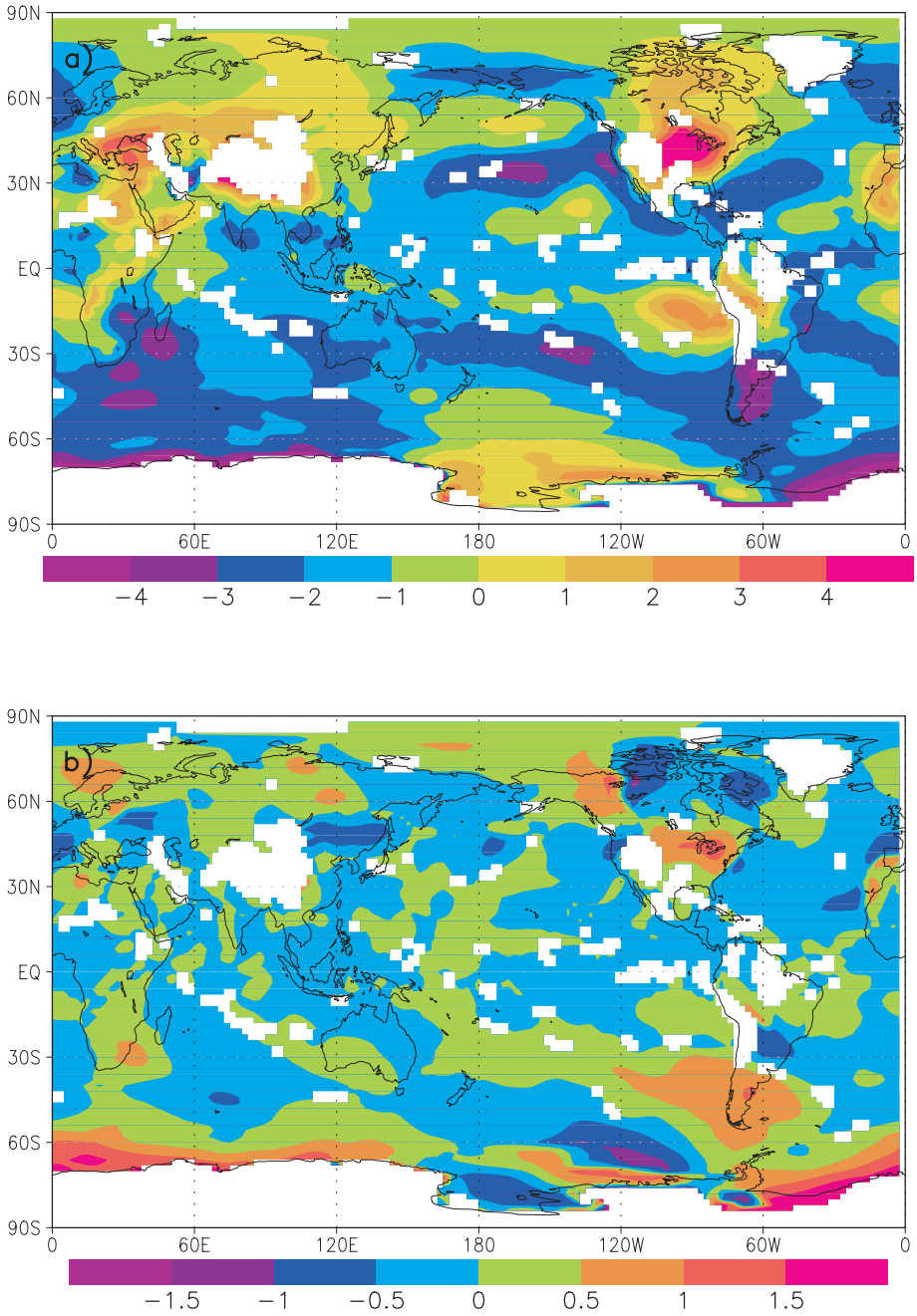

Fig. 1. June–July–August global temperature field at 850 mb in Kelvin. (a) Difference between model results using EM and observations, and (b) 'relative difference' (defined in the text) between simulations using EM and M and observations. Results that are not statistically significant and regions that are below topography at 850 mb are not shaded.

excursion of the monsoon precipitation over the land. The mechanism suggested for this behaviour was the lower boundary layer height in EM in the regions where the precipitation was higher. The lower boundary layer heights over wetter, cooler areas are associated with increased precipitation due to higher equivalent potential temperature. The precipitation over land and ocean in the region of the Australian monsoon will be presented to assess the possible improvement in the EM simulations of the monsoon.

A statistical assessment of the results presented here was performed. We regard the 10 yrs of our simulations with climatological SSTs as a ten-member ensemble of simulations because the year-to-year differences are due mainly to the differences in

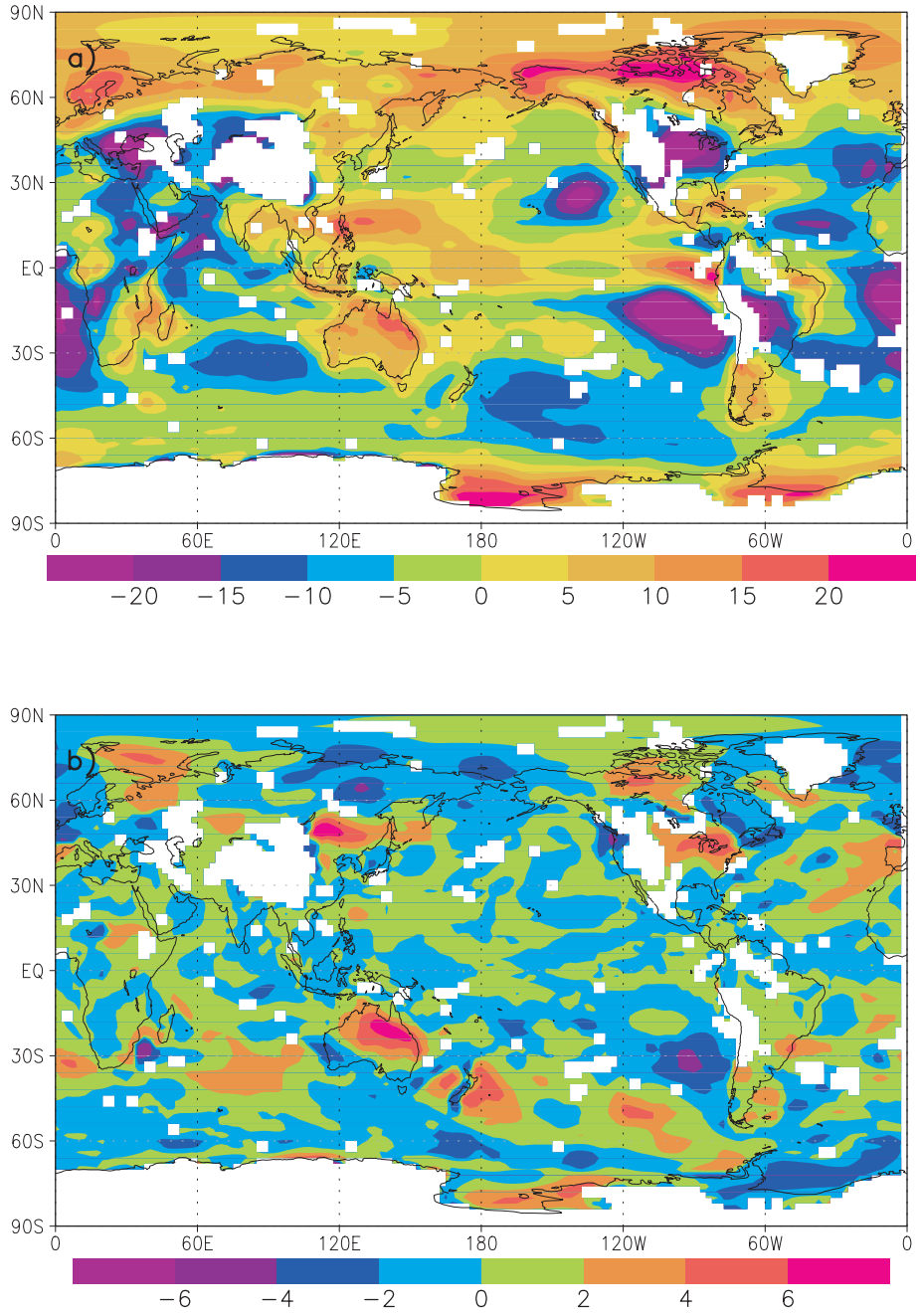

Fig. 2. June–July–August relative humidity at 850 mb. (a) Difference between model results using EM and observations and (b) 'relative difference' (defined in the text) between simulations using EM and M and observations. Results that are not statistically significant and regions that are below topography at 850 mb are not shaded.

atmospheric and soil state at the beginning of each year. We recognize that the presence of variability on scales greater than 1 yr would generate some correlation between the initial states of the ensemble members, but we assume that this does not affect the statistics of the ensemble. A Student's *t*-test was performed to assess the statistical significance of EM–M differences. All of the results that will be shown in this section are only shown over regions where EM–M differences are statistically significant with a confidence of 80% or more.

3.1. Summertime Climate

Figures 1, 2 and 3 show the Northern Hemisphere summer temperature in Kelvin and relative humidity in percent at 850 mb,

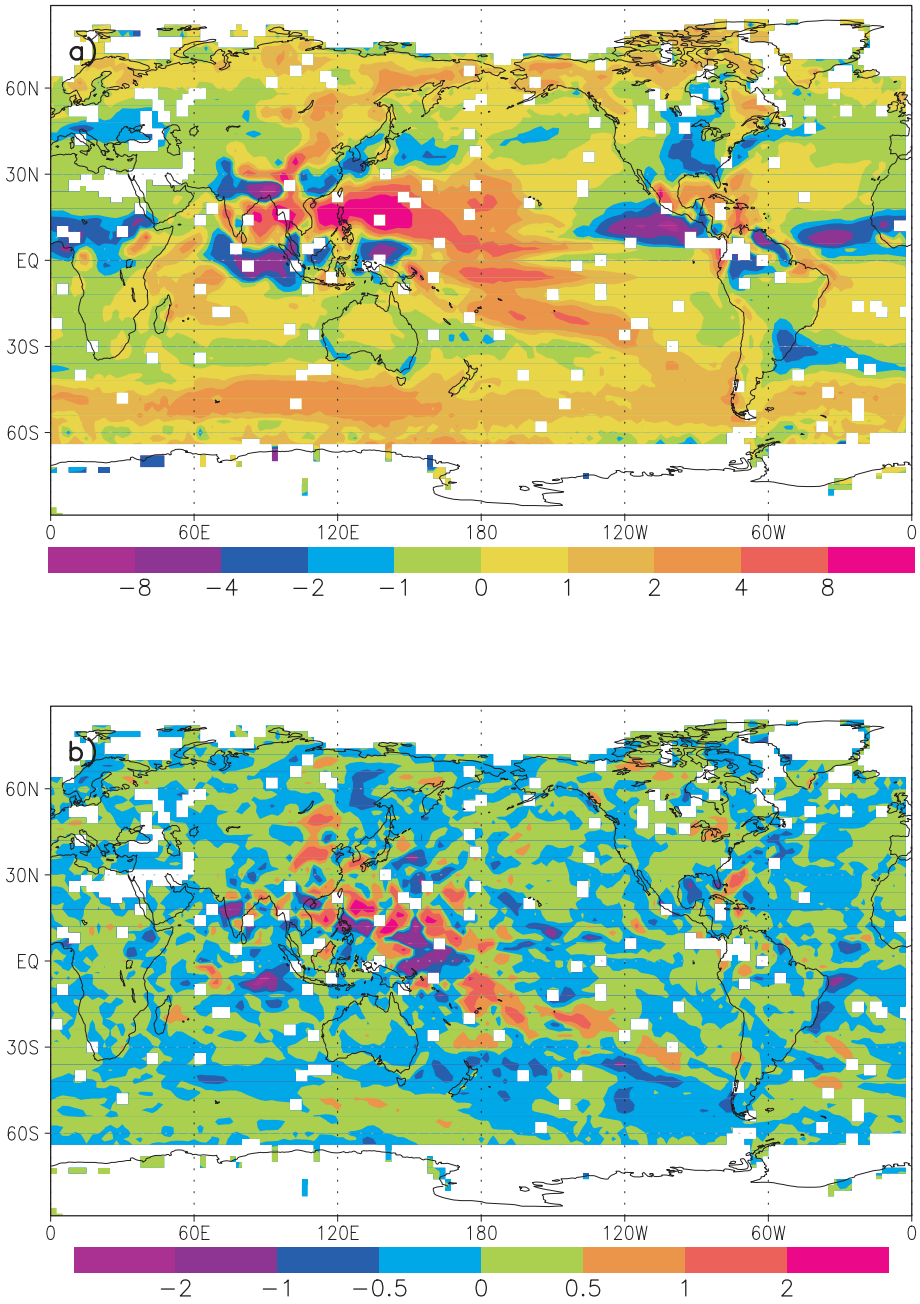

Fig. 3. June–July–August global total precipitation field. (a) Difference between model results using EM and observations and (b) 'relative difference' (defined in the text) between simulations using EM and M and observations. Results that are not statistically significant are not shaded.

and global total precipitation in millimetres per day, respectively. In each figure, panel (a) shows the 7-yr (the period of overlap between simulations and observations) actual difference between the EM simulation and observations, and panel (b) shows the 'relative difference' defined as $rd = |EM - OBS| - |M - OBS|$. The 'relative difference' is a measure of the difference between the simulation with EM and the observations *relative to* the difference between the simulation with M and the observations. Negative values of *rd* (blue shading) correspond to areas where climate simulations with EM are improved relative to climate simulations with M.

Figure 1a, the EM-OBS temperature difference at 850 mb, shows a general warm bias in EM summer hemisphere temperatures, with differences of up to 4 K over the central United States and eastern Europe. The winter hemisphere shows that EM is cold relative to observations. In Fig. 1b, the prevalence

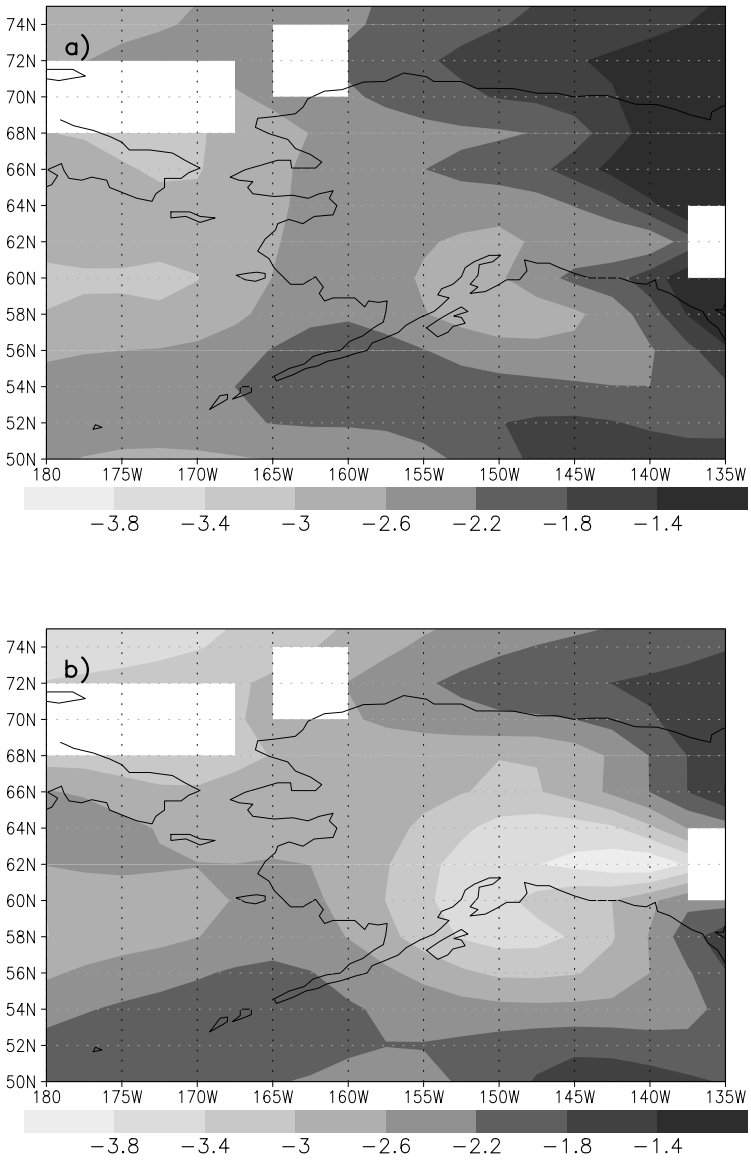

Fig. 4. December–January–February mean temperature at 850 mb field (in K) difference between simulations and data from NCEP/NCAR reanalysis over a northern Pacific area: (a) EM-reanalysis and (b) M-reanalysis. Contour levels are indicated in the colour-scale bar below each panel, the same shade of colours represents the same interval in both panels. Results that are not statistically significant and regions that are below topography at 850 mb are not shaded.

of the blue shading, which are negative values of *rd*, shows that the simulations with EM constitute an improvement over the temperatures obtained using the M scheme. The largest improvements are found over the central United States, central Eurasia and South Africa. There is also a region where EM is degraded relative to M over southern South America. The regions where the largest relative differences are found correspond to regions of high degree of surface variability and relatively weak summertime winds, which is consistent with the discussion of the impact of EM on the simulated climate presented in MSW04.

In Fig. 2, the 850 mb relative humidity EM-OBS difference and relative difference plots, we can see that the behaviour of the relative humidity at 850 mb over the United States corresponds directly to the behaviour of the temperature field; the drier relative humidity [blue in panel (a)] and the relative improvement of EM over M [blue shading in panel (b)] are associated with the warmer temperatures over this region. This correspondence, however, does not exist globally. Over South Africa, for instance, the colder temperature seen in the previous figure corresponds to a lower relative humidity, as seen in 2a. In addition, the lower relative humidity represents a degradation in EM relative to M, as shown by the yellow shading over South Africa in Fig. 2b.

Figure 3 shows global precipitation fields during the Northern Hemisphere summer season. There is little evidence of either large differences between EM and the observations or an improvement or degradation in the precipitation simulated with

EM over land, as can be seen from the low values of the difference in panel (a) or of *rd* in panel (b). Most of the differences are seen over ocean areas. Figure 3a shows excessive precipitation in EM over the western side of the ocean basins and not enough over the eastern side. This is consistent with errors in simulations of precipitation with many GCMs. Panel (b) shows that over the ocean there are as many regions of positive values of *rd* as there are of negative values, indicating that in general EM and M are similar as compared with observations.

3.2. Strength of the PNA

As an indicator of the strength of the PNA pattern in the northern hemisphere, Fig. 4 shows the 850 mb temperature over northwest Canada and Alaska during winter. Figure 4a shows the EM-Reanalysis difference, and indicates that the EM simulated temperatures are up to 3 K colder than the reanalysis. Figure 4b shows the M-Reanalysis difference, and shows differences that are up to 3.8 K colder than the reanalysis, indicating a degradation in the simulation with M of 0.8 K. The cold temperatures relative to the reanalysis implies that both simulations underestimate the strength of the PNA pattern. The results in Fig. 4 indicate that the underestimate is less severe in the GCM simulation with EM. Although the physical mechanism for strengthening of the PNA in the EM simulation is difficult to assess, it is feasible that a change in the precipitation pattern over the Asian continent could result in an increase in Rossby wave propagation over the Pacific, and so an increase in the PNA pattern strength.

3.3. Australian Monsoon

The difference among the EM and M simulations and observations of precipitation in the region of the Australian Monsoon can be seen in Fig. 5. Figure 5a shows the GPCP observational estimate, Fig. 5b shows the difference between the EM simulated precipitation and the observations, and Fig. 5c shows the 'relative difference', as defined above. The light grey shading over land (negative values) in panel (b), along with the dark grey shading (positive values) over the ocean, indicates that the excursion over land of the monsoon is underestimated in the EM simulation, and that excess precipitation occurs over the ocean. As indicated by the light grey shading in panel (c), the EM simulated precipitation represents an improvement over the M simulated precipitation over land. The dark grey shading in a small region to the north of the Australian continent in panel (c). indicates a degraded oceanic precipitation in EM simulations relative to M. The importance of the evaporation relative to sensible heat flux over the region of the Australian monsoon makes that a region where the impact of EM is to produce a wetter and cooler climate, according to MSW04. The increased excursion of the monsoon precipitation over the land, which constitutes an improvement in the simulated precipitation pattern, is a result of this impact.

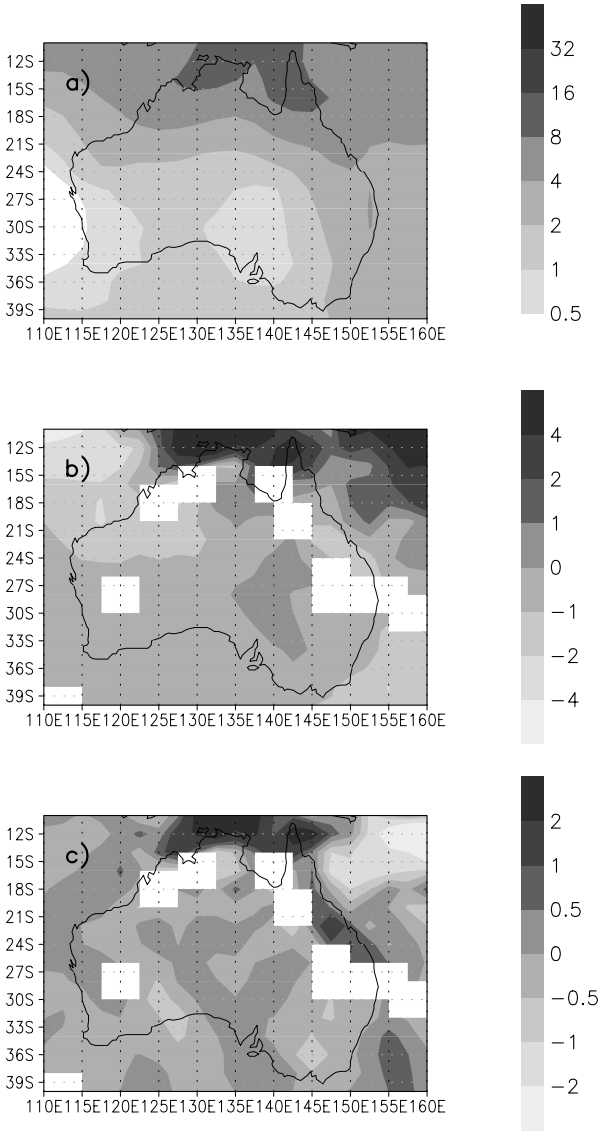

Fig. 5. December–January–February precipitation in mmday^{-1} over Australia. (a) Observed precipitation, (b) difference between simulations with EM and observations and (c) 'relative difference' (defined in the text) between simulations using EM and M and observations. Results that are not statistically significant and regions that are below topography at 850 mb are not shaded.

4. Summary

An evaluation of a set of GCM experiments which compares simulations using an EM technique to model the land–atmosphere coupling, the standard mosaic (M) technique, and observational estimates of climate was presented. The comparison focused on the regions where the largest statistically significant differences between simulations performed with EM and with M were found by a previous study (Molod et al., 2004). Seasonal mean fields for a 7-yr period (the period of overlap between simulations

and observations) from a set of 10-yr (1993–2003) simulations with each of EM and M were used for this comparison. Observational estimates for total precipitation data were derived from the satellite-gauge precipitation product of Huffman et al. (1995), and air temperature and relative humidity fields at 850 mb were evaluated using NCEP/NCAR reanalysis data (Kalnay et al., 1996).

The results presented in this work show that the model simulation using the EM technique results in improvements in air temperature and relative humidity at 850 mb over central United States and central Eurasia in summertime, and an improvement in the winter air temperature over South Africa. Further improvements include the winter air temperature over Alaska and Western Canada due to the strengthened amplitude of the PNA pattern of variability. In addition, using the EM technique results in an improved excursion of the Australian monsoon precipitation over land. Degradation in the EM simulation were seen in the relative humidity over South Africa in wintertime and in the temperature over southern South America in the winter.

5. Acknowledgments

The authors gratefully acknowledge partial funding for this work provided by the CUNY Research Foundation, PSC-CUNY Award No. 66304-00 35. The authors also wish to acknowledge the comments of anonymous reviewers, which led to improvements in the manuscript.

References

DeFries, R. S. and Townshend, J. R. G. 1994. NDVI-derived land cover classification at global scales. *Int. J. Remote Sensing* **15**, 3567–3586, Special Issue on Global Data Sets.

Dorman, J. L. and Sellers, P. J. 1989. A global climatology of albedo, roughness length and stomatal resistance for atmospheric general circulation models as represented by the Simple Biosphere model (SiB). *J. Appl. Meteor.* **28**, 833–855.

Huffman, G., Adler, R. F., Rudolf, B., Schneider, U. and Keehn, P. R. 1995. Global precipitation estimates based on a technique for combining satellite-based estimates, rain gauge analysis, and NWP model precipitation information. *J. Climate* **8**, 1284–1295.

Intergovernmental Panel on Climate Change (IPCC) 2001. Climate Change 2001: Synthesis Report. Contribution of working groups I, II and III to the Third Assessment Report of the International Panel on Climate Change. Cambridge Press, UK and New York, NY, USA.

Kalnay, E., Kanamitsu, M., Kistler, R., Collins, W., Deaven, D. and coauthors. 1996. The NMC/NCAR 40-Year Reanalysis Project. *Bull. Amer. Meteor. Soc.* **77**, 437–471.

Koide, H. and Kodera, K. 1999. A SVD analysis between the winter NH 500-hPa height and surface temperature fields. *J. Met. Soc. Japan* **77**, 47–61.

Molod, A., Salmun, H. and Waugh, D. W. 2003. A new look at modeling surface heterogeneity: extending its influence in the vertical. *J. Hydrometeorol.* **4**, 810–825.

Molod, A., Salmun, H. and Waugh, D. W. 2004. The impact on a GCM climate of an extended mosaic technique for the land-atmosphere coupling. *J. Climate* **17**(20), 3877–3891.

Reynolds, R. W. 1988. A real-time global sea surface temperature analysis. *J. Climate* **1**, 75–86.